STATE RESEARCH CENTER OF RUSSIA

INSTITUTE FOR HIGH ENERGY PHYSICS

REPORT

Preliminary Design Work on NBB Absorber and Target Prototype

(Task A of the Accord between FNAL and IHEP)

A.Abramov, I.Azhgirey, P.Galkin, N.Galyaev, V.Garkusha,
V.Ferapontov, A.Kharlamov, I.Kurochkin, E.Lomakin,
F.Novoskoltsev, A.Ryabov, V.Zapolsky, V.Zarucheisky

Protvino 1998

Contents

1 Beam Absorber for the Narrow Band Beam

The beam absorber is located in a narrow band beam (NBB) to absorb primary protons and the secondary particles being outside of useful beam, and to transfer their energy to the water cooling loop. Under the emergency situation, a few spills of the primary proton beam with full intensity should be absorbed without destruction of the absorber. This Section presents a first approach to the beam absorber design based on the results of energy deposition calculations taking into account the real geometry and equipment parameters of the NBB.

1.1 General Description of the Beam Absorber

The location of the beam absorber in the beam line is shown in Figure 1.1. For the preliminary design work the graphite part of the absorber was chosen 2.4 m in length ($4.8\lambda_c$) and 177 mm in diameter, as shown in Figure 1.2. The diameter of a graphite core was determined by the possible positions of a proton beam for different tunes of the NBB, as well as the neutral direction from the target. The graphite core is held in a water cooled aluminum jacket with the sizes shown in Figure 1.2. The length of aluminum along the beam is equal to 0.85 m ($2.2\lambda_{Al}$) and is limited by the location of the NBN magnet (see Figure 1.1), whereas the transversal size of the aluminum jacket is limited by the useful beam dimensions and is equal to 250 mm. A light shrinkfit (0.06 mm) is necessary to insure good thermal contact between the graphite cylinder and the aluminum jacket. The graphite and aluminum were chosen the same as in the beam absorber corebox for the FNAL Main Injector Abort System [1],[2].

In order to prevent oxidation of the graphite, a 0.15 mm thick titanium window seals and separates the graphite cylinder in dry nitrogen environment.

The cooling system has 8 water channels with a total flow rate of 106.4 l/min (28 gpm) in four parallel paths through the aluminum section of the corebox. The diameter of each water channel is equal to 12.7 mm

(1/2"), the water velocity is chosen of 3.5 m/sec which corresponds to the heat transfer coefficient of 12 kW/m^2/K. The pressure drop is equal to 1.345 atm (1.99 psi).

1.2 Incident Energy Characteristics in front of the Absorber

The investigation of particle distributions in front of the absorber, as well as calculation of the energy deposition in the absorber corebox, has been carried out using the Monte Carlo computer code MARS'96 [3], which simulates the three dimensional hadron and electromagnetic cascades, taking into account the real geometry of narrow band beam line.

The NBB graphite target with 4 mm in diameter has the length of 50 cm ($\sim\lambda_c$). Focusing device FD1 is an assembly of two bolted together parabolic lenses with feeding current of 320 kA. The real field map in the NBR magnets is computed by program POISSON and is taken into account in beam simulations as well as the magnetic field in FD1.

The incident energy density distribution in front of a corebox for the 45 GeV/c NBB tune, normalized to one primary proton is shown in Figure 1.3. The origin of coordinate system ($x = y = 0$) corresponds to the wide band beam (WBB) axis, the axes directions are shown in Figure 1.2b. The peak of energy density distribution is 23.7 cm lower of the WBB axis in Y–direction. It corresponds to the position of primary proton beam. The Y–coordinate equaled to 16 cm corresponds to the beginning of the useful beam aperture. The full width of the energy density distribution along the X–direction is determined by the NBR magnets gap and is equal approximately to 10 cm. The parameters of the incident beam in front of the absorber are given in Table 1.1.

Maximum particles energy	120 GeV
Total kinetic energy in a beam	0.407 MJ
Kinetic energy of primary protons	0.321 MJ
Kinetic energy of secondaries (p,$\pi^{\pm}$,$\pi^{\circ} \rightarrow 2\gamma$)	0.086 MJ
Pulse duration	1.0 msec
Repetition period	1.9 sec
Average beam power	215 kW

Table 1.1: Beam parameters in front of the absorber corebox.

The hardest situation for the beam absorber arises when the target is out of primary proton beam. In this case a few spills of the primary proton beam with the parameters given in Table 1.2 should be absorbed without destruction of the beam absorber.

Beam energy	120 GeV
Total kinetic energy	0.768 MJ
Pulse duration	1.0 msec
Short term continuos operation	1 or 2 spills
Number of protons per spill	$4{\cdot}10^{13}$
Transverse beam size (Gaussian beam distribution), $\sigma_x = \sigma_y$	1.1 mm

Table 1.2: Primary proton beam parameters in front of the absorber corebox with the target out of the beam.

1.3 Energy Deposition in the Absorber Corebox

The energy deposition was calculated on a per grid zone basis. The transversal zone size varies from 0.25 cm near the beam axis to 1.0 cm at the outer perimeter. Along the azimuthal axis, Δz is alternated with 3 cm and 30 cm. The origin of coordinate system for energy deposition calculations corresponds to the corebox axis with X–axis having direction to the right and Y–axis down.

The distribution of maximum energy deposition density along the proton beam axis given in Figure 1.4 has two peaks at $z = 34.5$ cm (graphite part of a corebox) and at $z = 252$ cm (aluminum). The first peak has the value of $7{\cdot}10^{-3}$ GeV/cm^3 and the second one $\sim 2.2{\cdot}10^{-3}$ GeV/cm^3 per one primary proton. The transversal distribution of energy deposition density at $z = 34.5$ cm (see Figure 1.5) is practically symmetric in the X–direction whereas in the Y–direction the distribution is non–symmetric with the peak at $y \simeq -5$ cm which corresponds to the position of primary proton beam for the 45 GeV/c NBB tune. Similar situation takes place at $z = 252$ cm (see Figure 1.6).

The results of the MARS'96 simulations of the energy deposition for the preliminary design of the absorber corebox are summarized in Table 1.3.

Total deposited energy	0.208 MJ
Total absorbed power	110 kW
Emitted energy:	
hadrons from lateral surface	0.091 MJ
gammas from lateral surface	0.067 MJ
hadrons from the back end	0.024 MJ
gammas from the back end	0.0013 MJ

Table 1.3: Deposited and emitted energy in the corebox.

1.4 Temperature and Stress Analysis

The temperatures and stresses in the absorber corebox have been computed by finite element program HAST [4], using the energy deposition distributions obtained from MARS'96 simulations. The steady states in the points, corresponding to the maximum energy deposition densities along the beam for graphite ($z = 34.5$ cm) and aluminum ($z = 252$ cm), are reached in 100 and more than 120 pulses respectively, as shown in Figures 1.7 and 1.8. The maximum temperatures are equal to 80.6°C in graphite and 81.5°C in aluminum. The distributions of temperature along Y–axis ($x = 0$) for both cases are shown in Figures 1.9 and 1.10.

For the preliminary design of a corebox the stress estimations have been made in two dimensional approach, taking into account the preloading caused by a light shrinkfit (0.06 mm). The thermal stresses in the cross section, corresponding to $z = 34.5$ cm are shown in Figure 1.11. The maximum equivalent stress (S_{eq}) is reached in aluminum near the water channels and is equal to $\sim$19 N/mm^2. The equivalent stress at $z = 252$ cm reaches also its maximum value of $\sim$49 N/mm^2 at the positions corresponding to the water channels in aluminum jacket (see Figure 1.12). For comparison, the aluminum alloy 5083–H112 has yield strength of 193 N/mm^2 and fatigue strength of 158 N/mm^2 ($5 \cdot 10^8$ cycles).

Figures 1.13 and 1.14 give the stresses along the contact line between graphite and aluminum at $z = 34.5$ cm. The shape of curves reflect the structure of the cooling system. As follows from these Figures, the S_{rr} stress in graphite is negative, i.e. it is compressed and good thermal contact between graphite and aluminum is not lost due to the beam heating.

1.5 Conclusions

Preliminary design of the absorber corebox shows that the lengths of graphite and aluminum are not quite optimal. The relatively small temperatures (and consequently thermal stresses) in graphite and aluminum allow to decrease the length of the graphite and aluminum parts of the absorber and correspondingly to have a lower cost of the absorber.

The total energy emitted from the back end of the corebox reaches the value of 0.0253 MJ and irradiates the NBN magnet coils. Estimations show that at such energy flux the absorbed doze in the NBN magnet coils will reach of 10^8 Gy/year. In order to decrease this energy flux, the length of the absorber should be increased by additional iron block with the length of about 1.4 m placed behind aluminum.

Further considerations shall be made to optimize the length of graphite, aluminum and iron taking into account the real distributions of incident beam energy in front of an absorber, as well as the emergency situation when the whole primary proton beam strikes on a corebox.

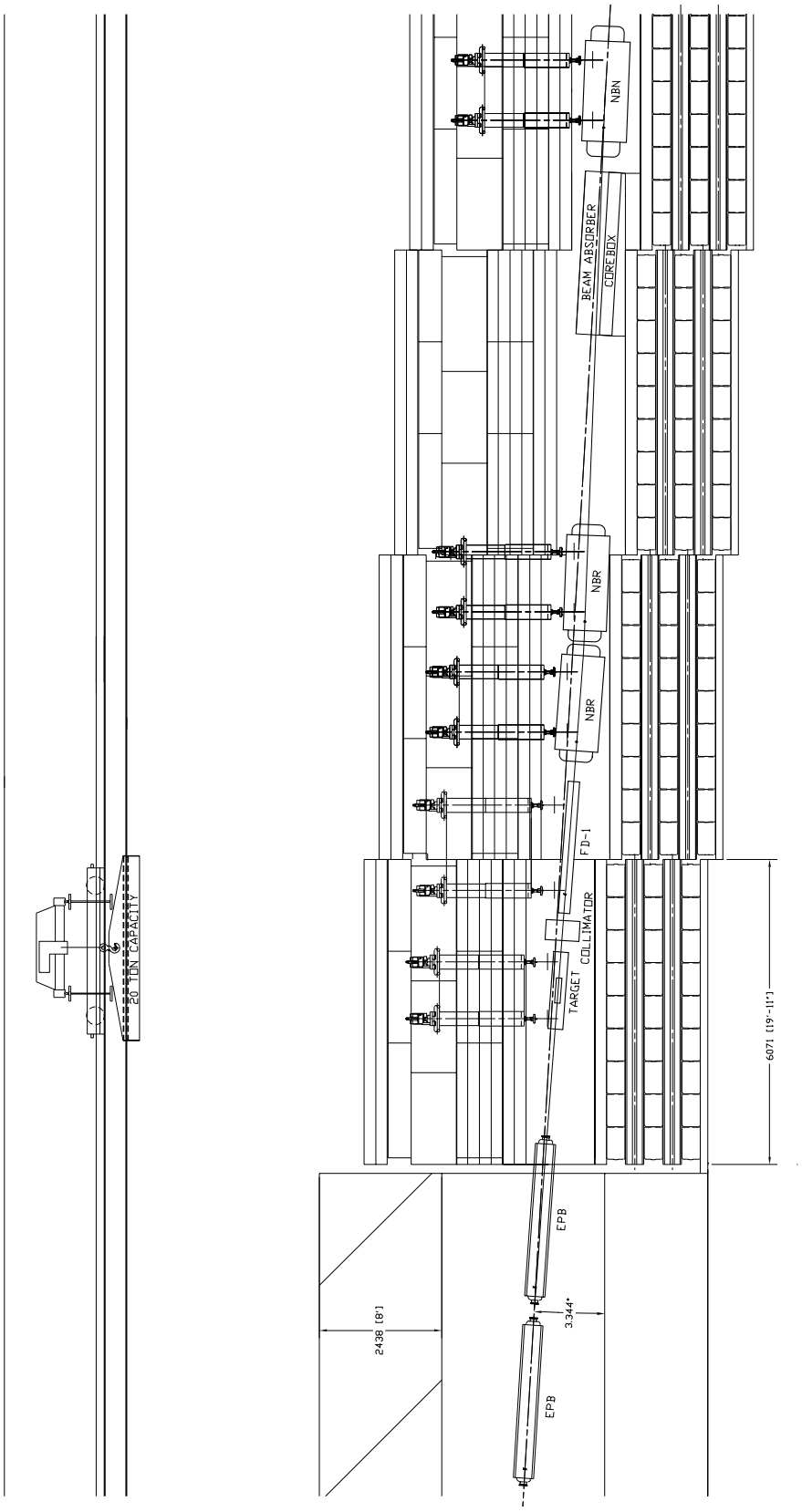

Figure 1.1: The layout of the NBB.

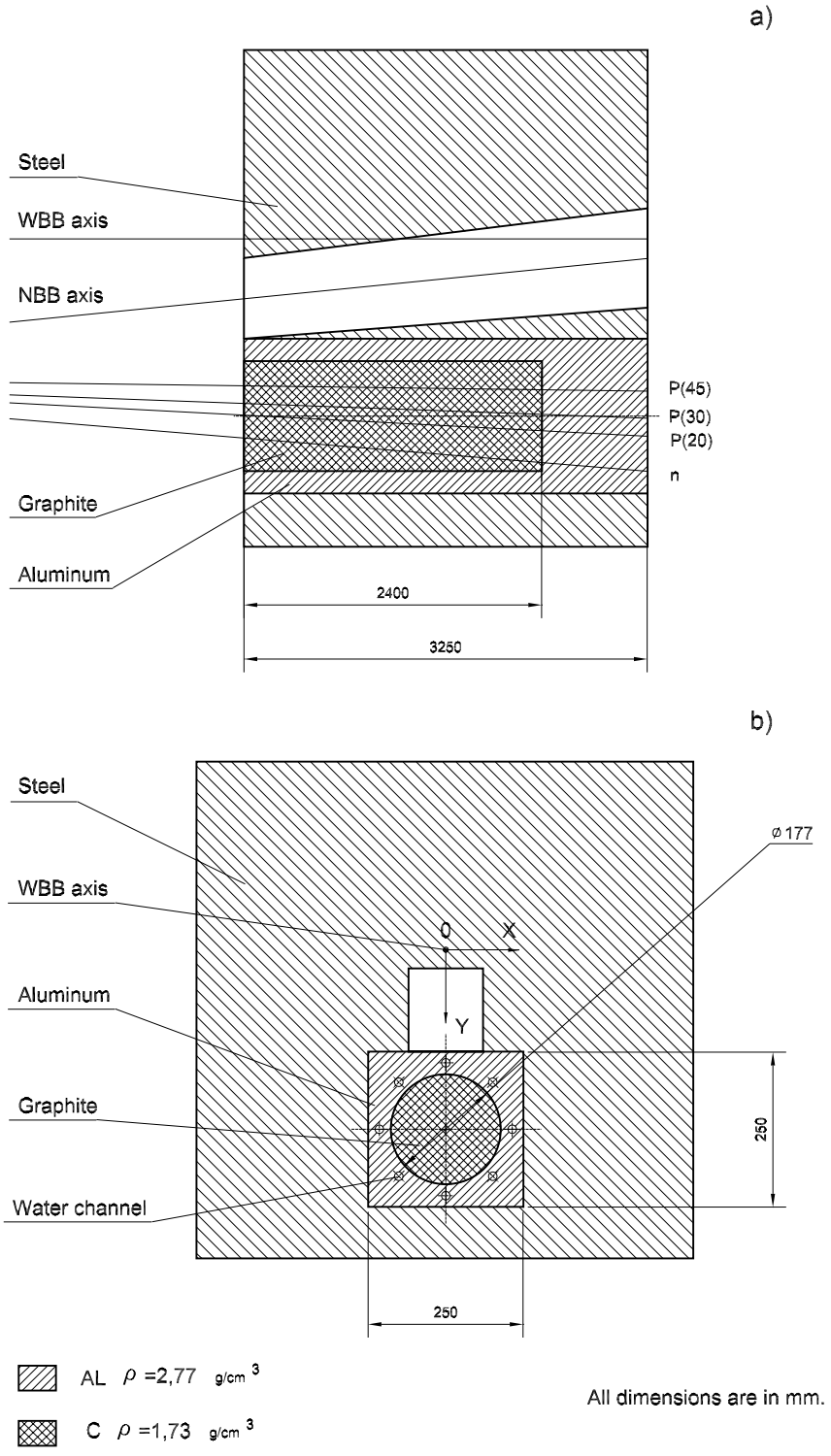

Figure 1.2: Longitudial (a) and transversal (b) cross-sections of the NBB absorber.

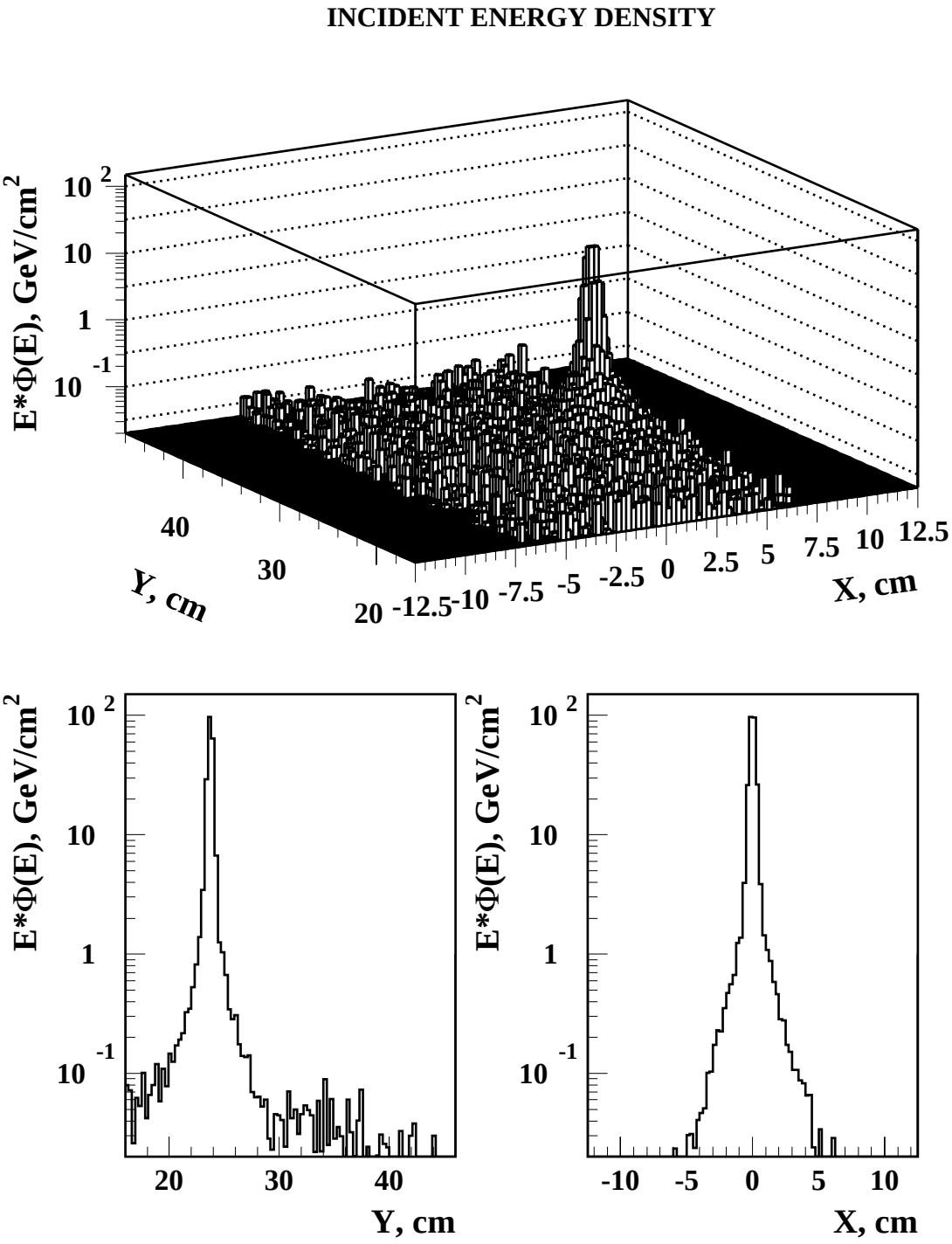

Figure 1.3: The incident energy density in front of the corebox.

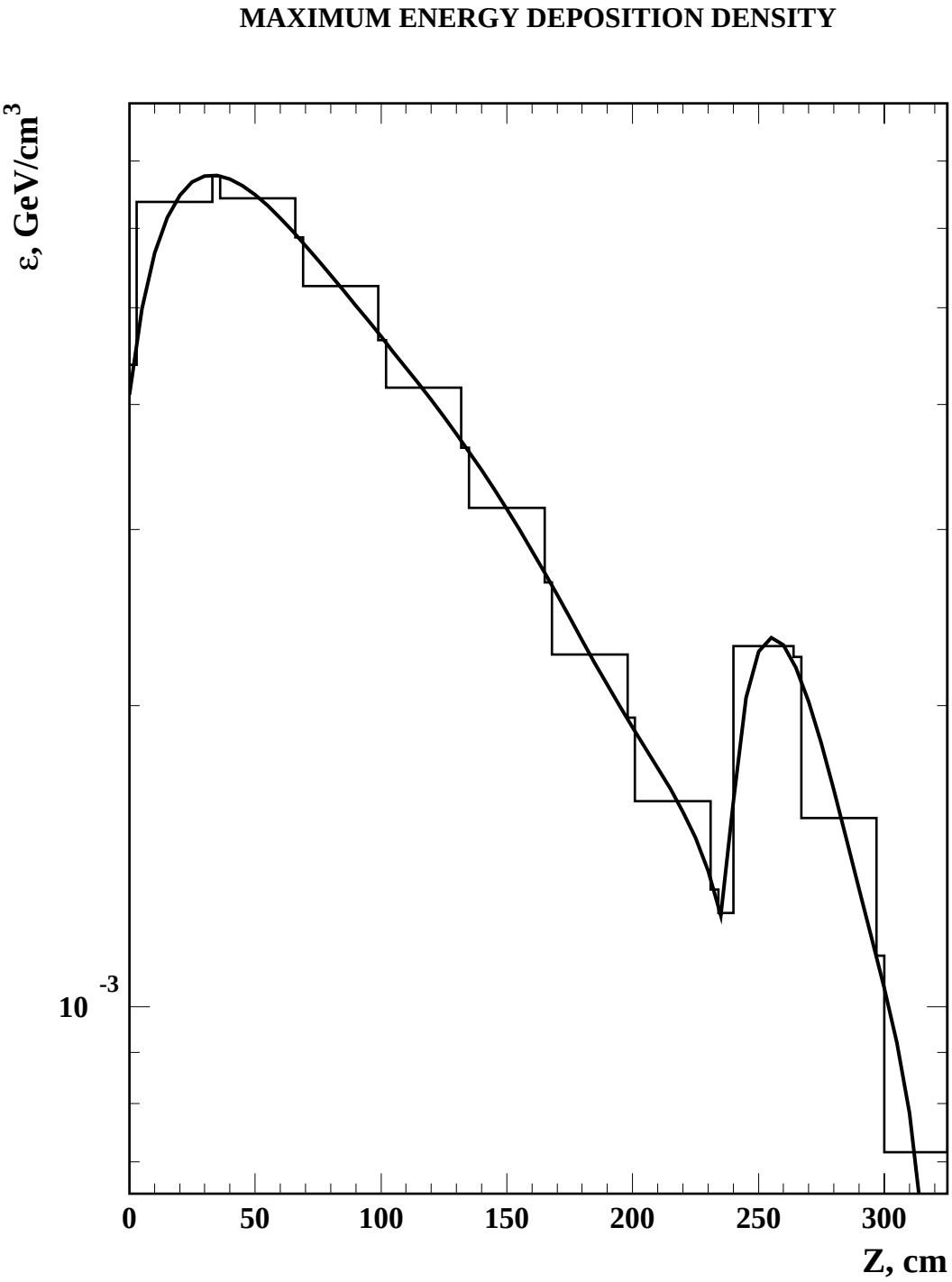

Figure 1.4: The longitudinal distribution of the maximum energy deposition density.

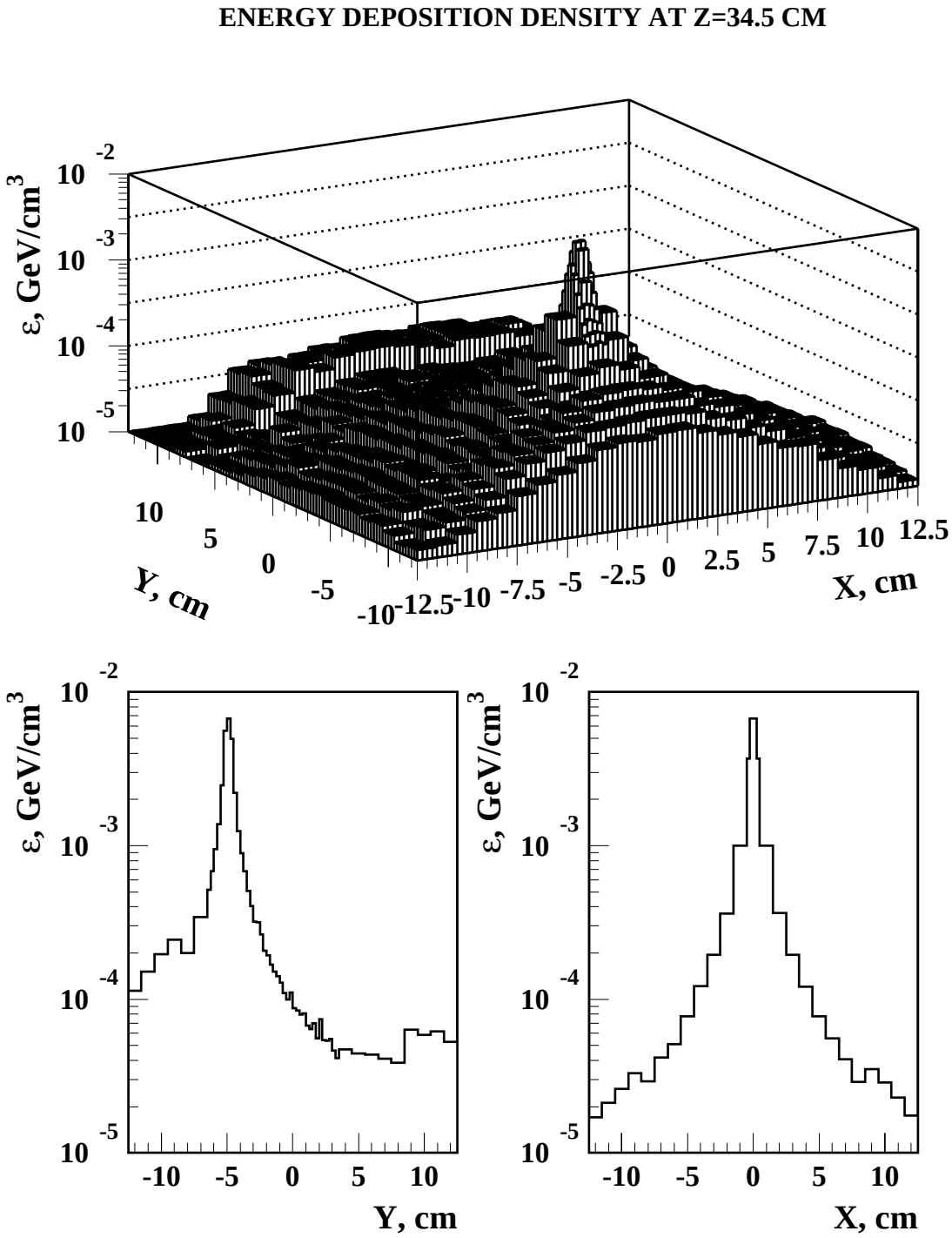

Figure 1.5: Transversal distribution of the energy deposition density in the corebox at $z = 34.5\,\mathrm{cm}$.

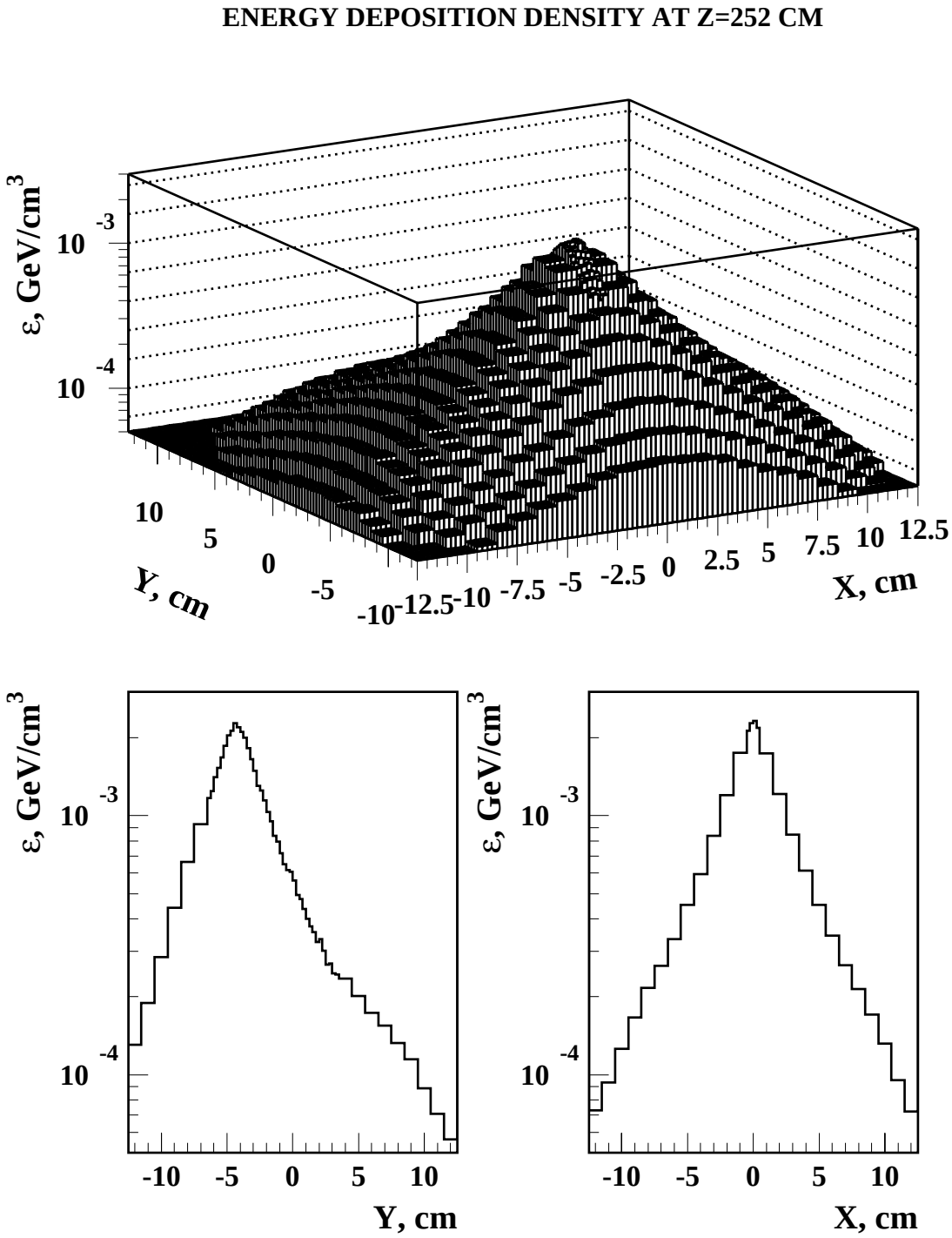

Figure 1.6: Transversal distribution of the energy deposition density in the corebox at $z = 252\,\mathrm{cm}$.

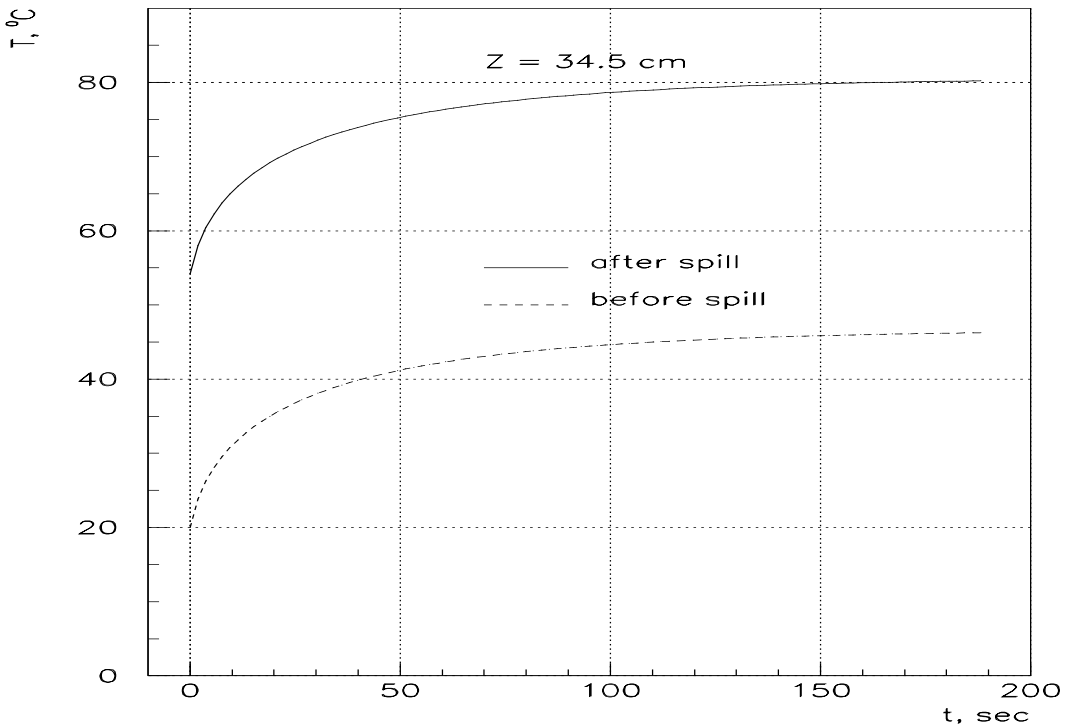

Figure 1.7: Evolution in time of the maximun and minimum temperatures in graphite.

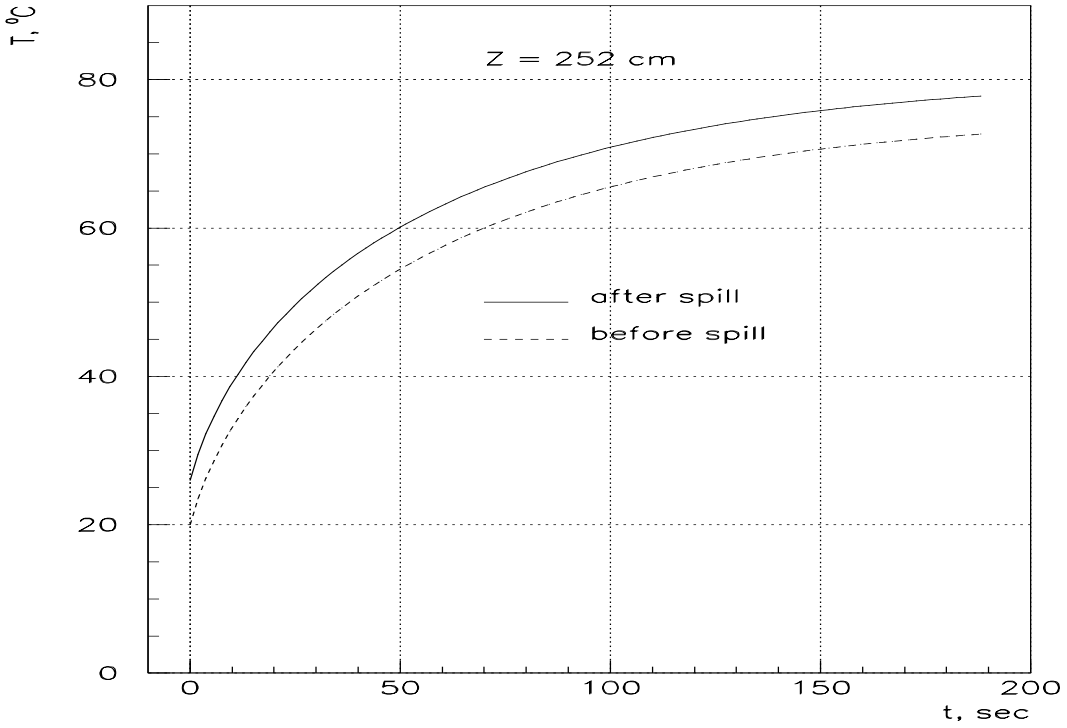

Figure 1.8: Evolution in time of the maximun and minimum temperatures in alumimun.

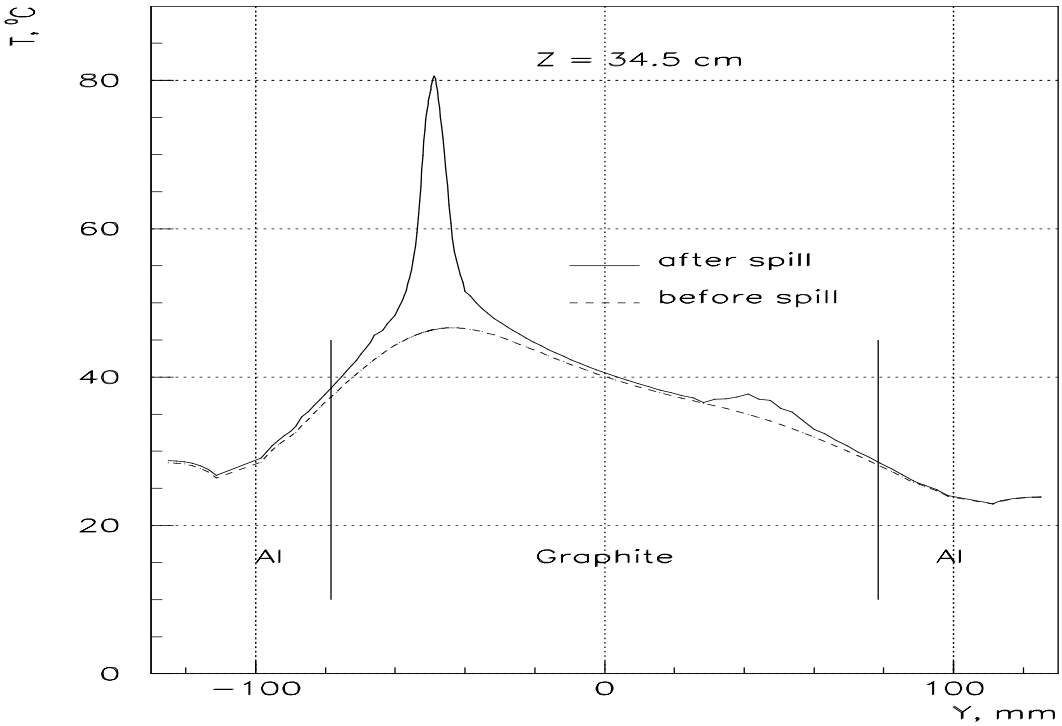

Figure 1.9: Temperature distribution along the Y–axis (x = 0) in graphite.

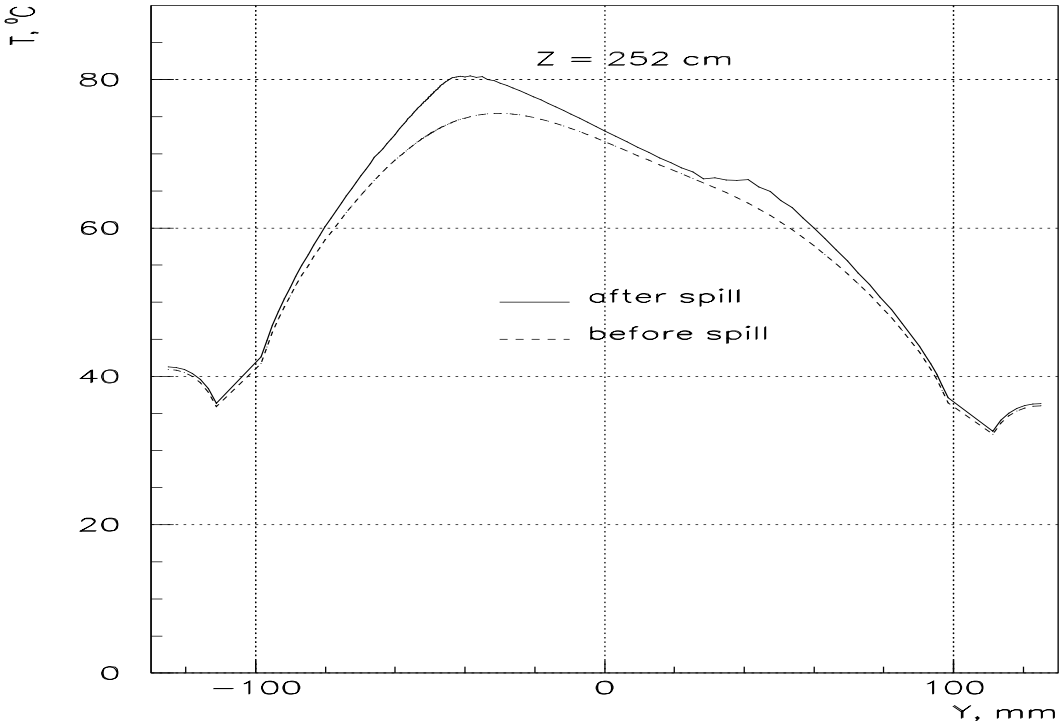

Figure 1.10: Temperature distribution along the Y–axis (x = 0) in aluminum.

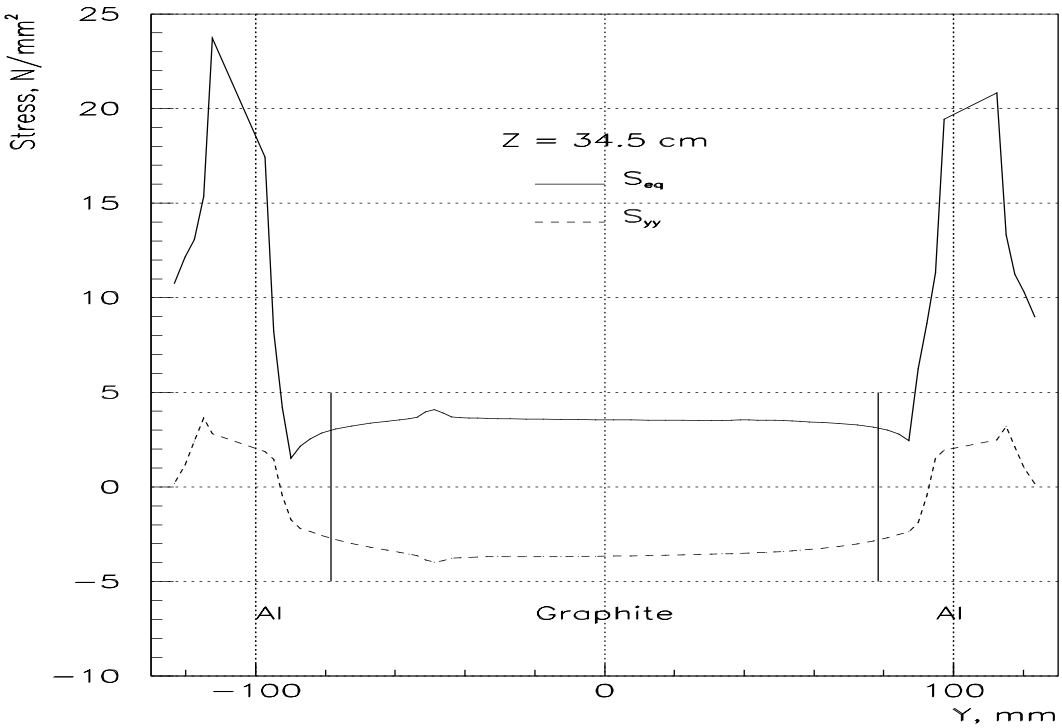

Figure 1.11: Stresses along the Y–axis (x = 0) in graphite.

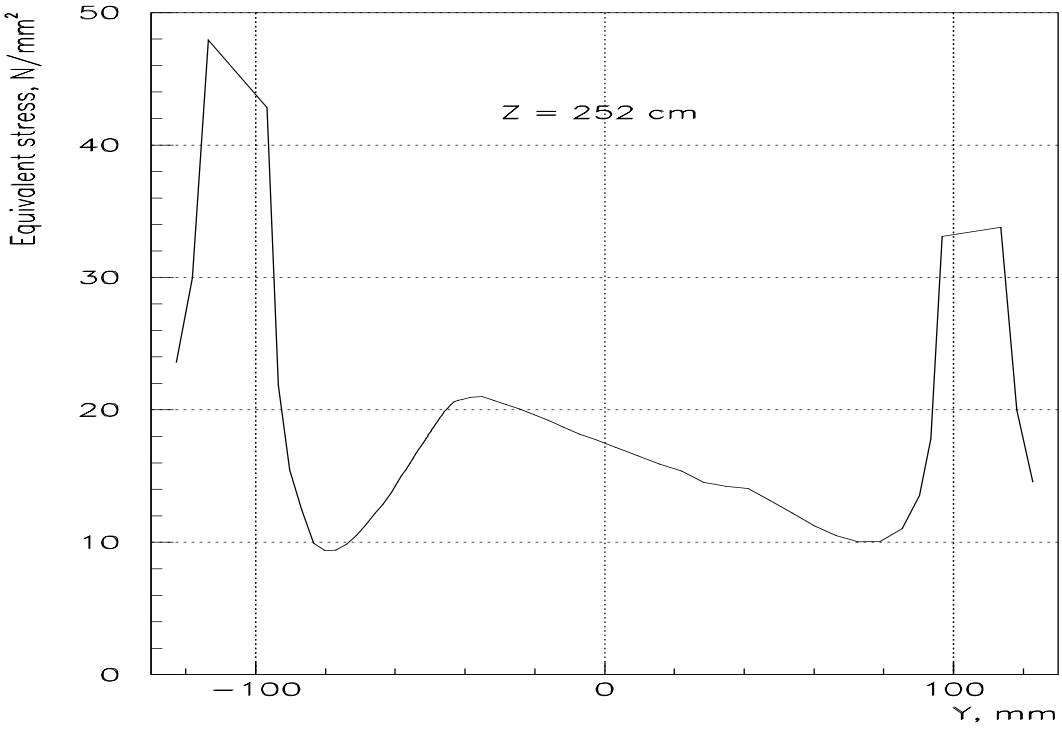

Figure 1.12: Equivalent stress along the Y–axis (x = 0) in aluminum.

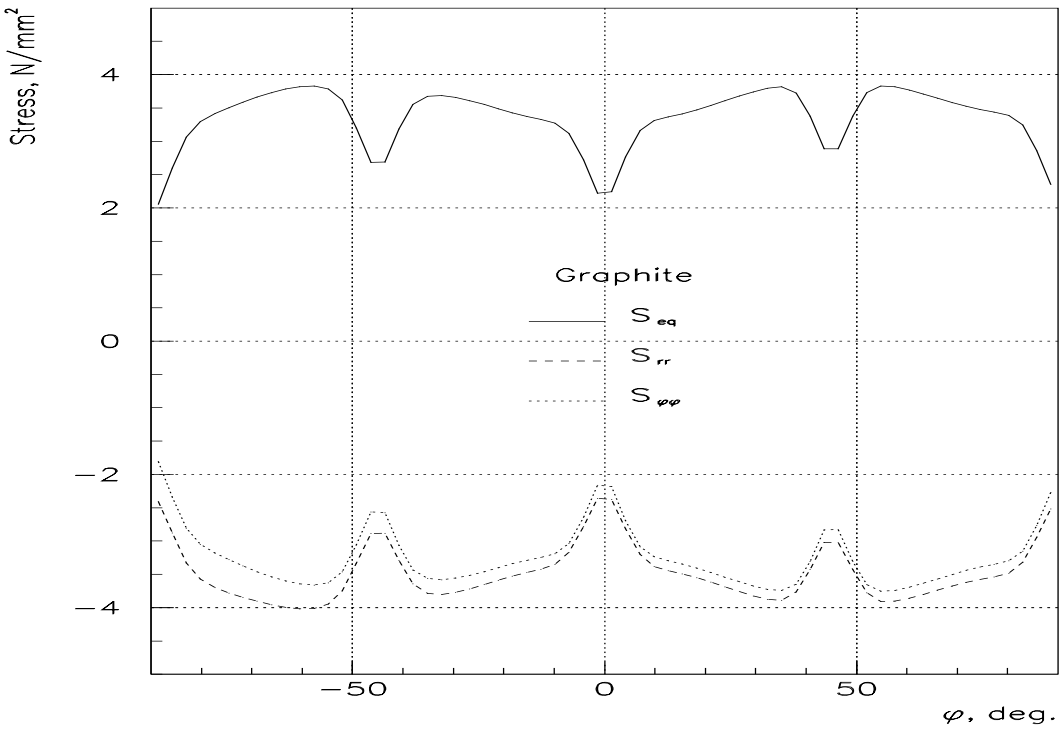

Figure 1.13: Stresses in graphite at z = 34.5 cm along the contact line between graphite and aluminum.

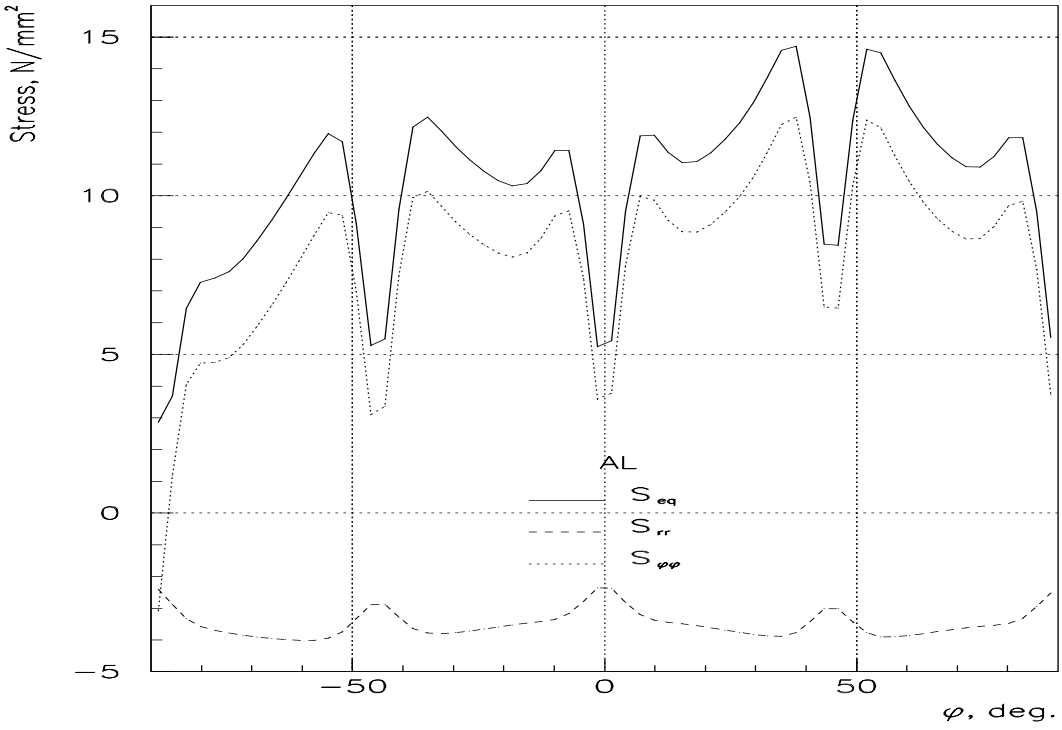

Figure 1.14: Stresses in aluminum at z = 34.5 cm along the contact line between graphite and aluminum.

2 Target Prototypes

The target prototypes should reflect the main peculiarities of the full scale beryllium and graphite water cooled fin targets. It means that prototypes, if it is possible, should have:

- the same temperature distributions;
- the same thermal stresses (or the same safety factor);
- water cooling system and mechanical support system;
- charge monitoring of the target ("Budal").

Additionally, the prototype design should have special glass window to look at the target surface after the testing. The main problem in a target prototype design is the essentially different operating conditions for the full scale target and the target prototypes (see Table 2.1).

Targets	Full scale	Prototypes
Type of beam	NuMI beam	Test beam
Beam energy	120 GeV	120 GeV
Number of protons per spill	$4{\cdot}10^{13}$	$5{\cdot}10^{12}$
Total kinetic energy	0.768 MJ	0.096 MJ
Pulse duration	1.0 msec	10 μsec

Table 2.1: Operating conditions of the targets.

2.1 Target Prototype Preliminary Design

The target prototype preliminary design is shown in Figures 2.1 and 2.2. Conventionally, the thickness of beryllium target segment is equal to 4 mm in order to see it well at small scale sketch. Beryllium target segment is pressed between aluminum base plate and aluminum pressing plate (Figure 2.2). The vertical position of a target segment is fixed by two small ceramic cylindrical pins. The base plate is clamped to the mounting plate (Al) by means of four screws.

Cooling water passes through the stainless steel pipes with inside diameter of 10 mm. A small shrinkfit is necessary between the pipes and aluminum plates in order to provide a good thermal contact. The machining of both plates should be produced with inserted pipes. Each of the aluminum details is anodized by alumina (40 μm thick) in order to provide insulation of target segment for "Budal" monitor. Several flexible bellows are used in order to make easy an assembly of target unit and to protect the base and pressing plates from any forces arised in a design.

The mounting plate with all details assembled on it is inserted into stainless steel tube and is clamped to two plates, welded to the internal surface of stainless steel tube. Two flanges with two titanium windows separate the internal volume from surrounding environment. The sizes of titanium windows are the same as in the full scale target.

2.2 Estimations of the Test Beam Spot Size and the Target Prototype Segment Size

The estimations of the test beam spot size and the target prototype segment size have been carried out for beryllium target to work out a criterion of similarity. The number of particles per spill in the test beam is 8 times less than in NuMI beam (see Table 2.1). So, in order to provide the same energy deposition density in a prototype as in a full scale target, the density of protons in the first approach should be increased 8 times. For beryllium fin target, operating with the proton beam spot size $\sigma_{\rm x} = 1.0$ mm and $\sigma_{\rm y} = 2.0$ mm, the maximum energy deposition density is equal to 0.0312 GeV/g per one proton. It means that for the test beam the maximum energy deposition density should be about 0.250 GeV/g/proton.

The maximum energy deposition densities near the beam axis in beryllium cylindrical target as functions of the proton beam spot sizes are listed in Table 2.2 (data obtained by the computer code MARS13 [5]).

Proton beam spot size, $\sigma_{\rm x} = \sigma_{\rm y}$, mm	0.3	0.4	0.5	0.7	0.8	0.9
Energy deposition density, GeV/g/proton	0.54	0.32	0.21	0.11	0.08	0.07

Table 2.2: Energy deposition density in Be cylindrical target.

As follows from this Table, the test beam spot size should be of $\sigma = 0.4 \div 0.5$ mm. The MARS13 simulations for the beryllium fin target with $\sigma_y \approx 2\sigma_x$ show that the energy deposition density of 0.270 GeV/g/proton is reached in the test beam with $\sigma_x = 0.33$ mm and $\sigma_y = 0.66$ mm. In this case the thickness of the target prototype segment should be 1.32 mm, with the proton beam axis being at 1.34 mm from the upper end of the target segment.

2.3 Temperature and Quasistatic Thermal Stress Analysis

The temperature and quasistatic thermal stresses have been computed by program HAST [4] using the distributions of energy deposition density obtained by MARS13 for the target prototype segment size and the proton beam spot size mentioned above.

HAST simulations show that it is practically impossible to realize the maximum temperature of the full scale target ($T_{max} = 202°C$ at film coefficient to water of 10 kW/m^2/K) in the target prototype due to a relatively low power ($\sim$50 W) absorbed in the prototype. In the full scale target the absorbed power in the second segment has the value of $\sim$350 W. For the target prototype located in vacuum box with the film coefficient to cooling water of 2.5 kW/m^2/K the maximum temperature at steady state reaches 165°C. Decreasing the film coefficient leads to a very high temperature constant of the target.

The beryllium segment of the target prototype under the cooling conditions, mentioned above, reaches the steady state in about 40–50 pulses, as shown in Figure 2.3. The temperature distributions along the target vertical axis before and after a spill in steady state are shown in Figure 2.4 (point $x = y = 0$ corresponds to the position of the proton beam axis). The adiabatic temperature jump ΔT is equal to 95°C (for full scale target $\Delta T = 85°C$).

Only the quasistatic thermal stress has been computed for the preliminary considerations. The dependencies of equivalent stresses in the target subsegment as functions of its length L are shown in Figure 2.5. Points 1 and 2 have (0;0;0) and ($\pm$d/2;0;0) coordinates with respect to the subsegment center respectively, where d is the subsegment thickness.

The minimum stress is equal to 130 MPa and corresponds to the optimal length of subsegment of $\sim$3.0 mm. For comparison the similar stresses for

the full scale target are shown in Figure 2.6. As one can see, the quasistatic stresses for the target prototype and the full scale target are equal. It confirms that the chosen method of similarity between the full scale target and its prototype is quite correct.

2.4 Conclusions

In conclusion it is necessary to note that the full analysis of the stresses in a target prototype should be done taking into account the dynamic thermal stress. It will be done by ANSYS computer code, because program HAST may compute only static stresses.

Further considerations shall be made to estimate the test beam spot size and the target prototype segment size for graphite target after the completion of the full scale graphite target optimization.

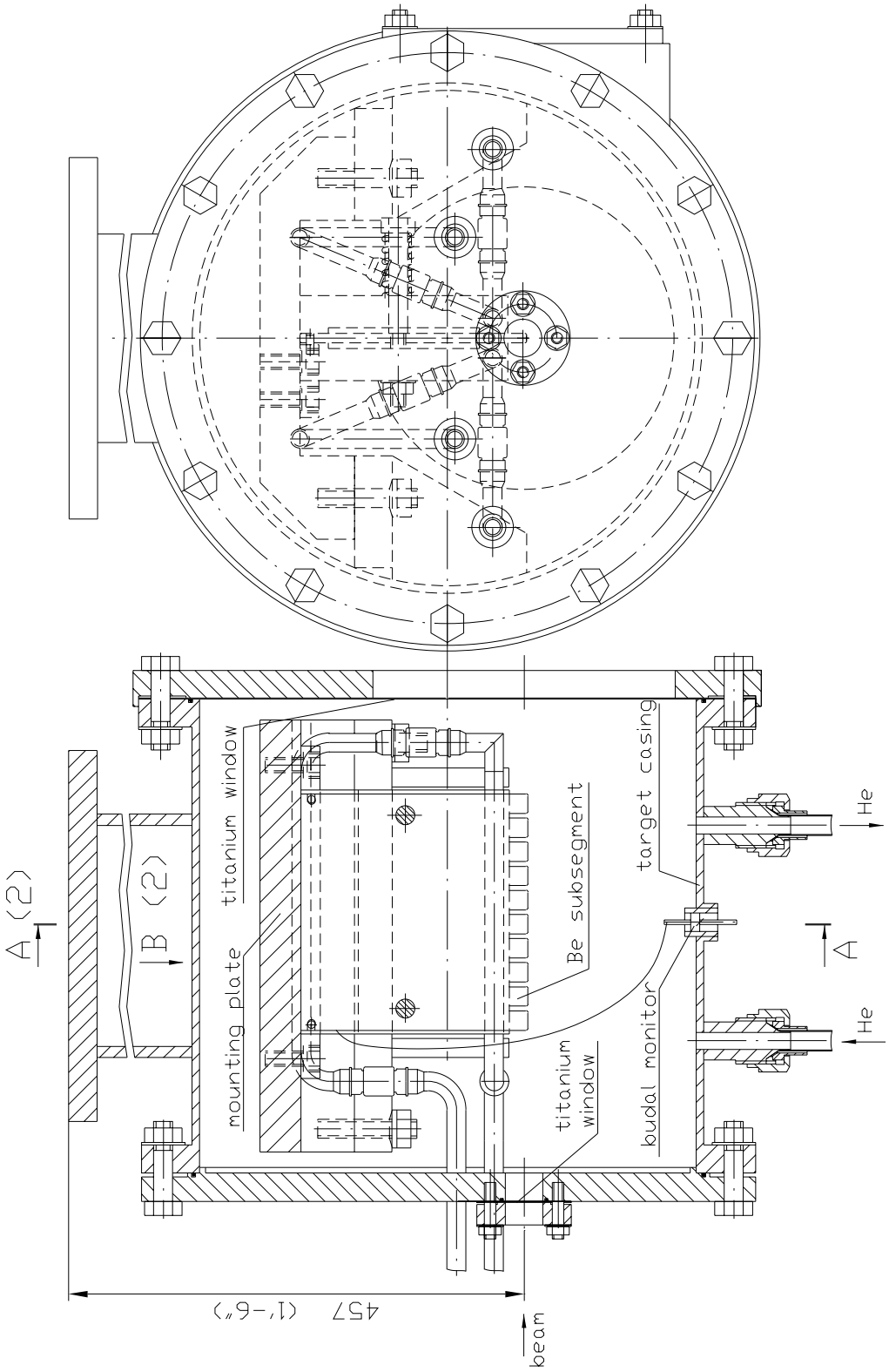

Figure 2.1: The target prototype module with Be fin segment.

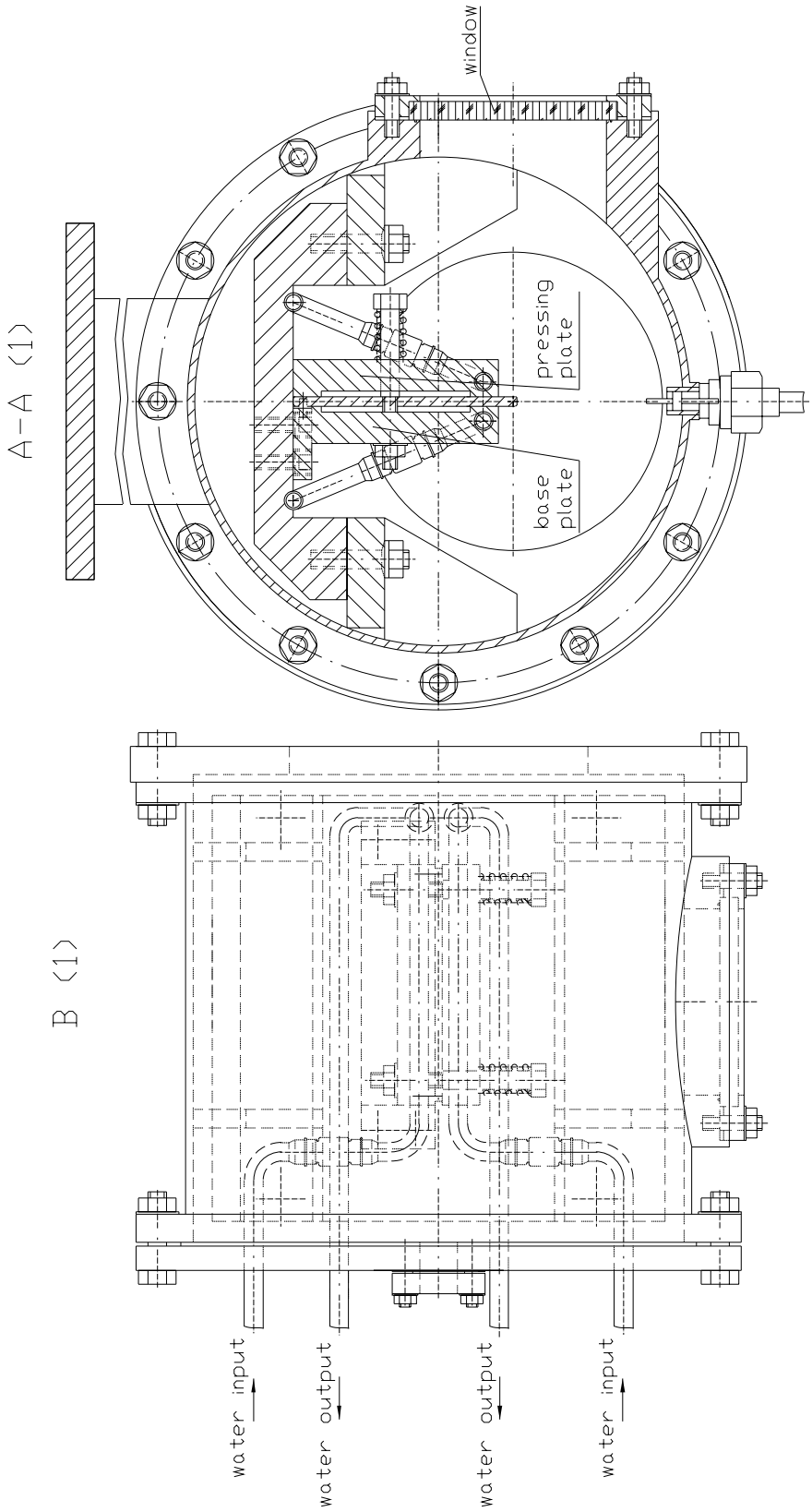

Figure 2.2: The top (B) and cross-section (A–A) views of the target prototype module shown in Figure 2.1.

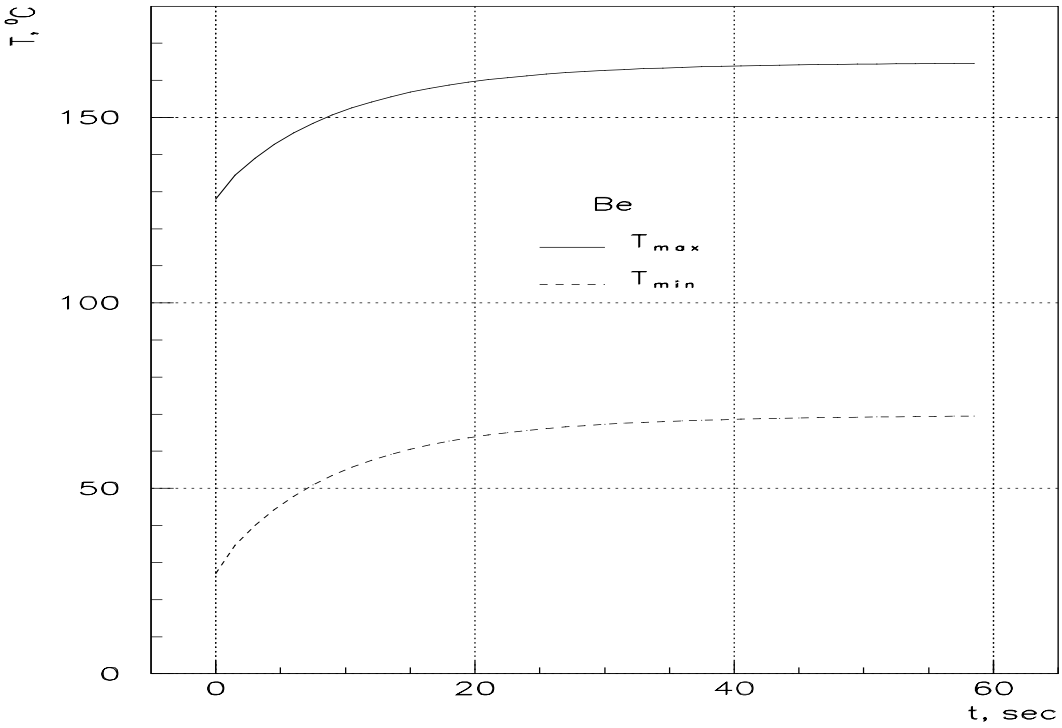

Figure 2.3: The evolution in time of maximum and minimum temperatures for the Be target prototype.

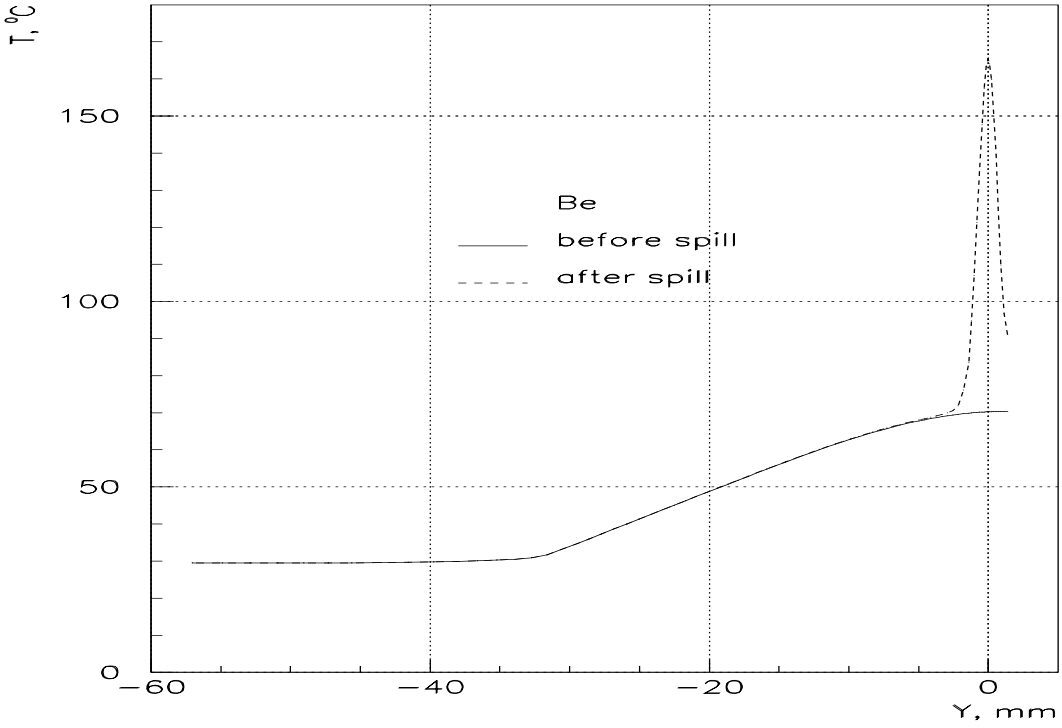

Figure 2.4: Temperature distributions in the target segment along Y–axis.

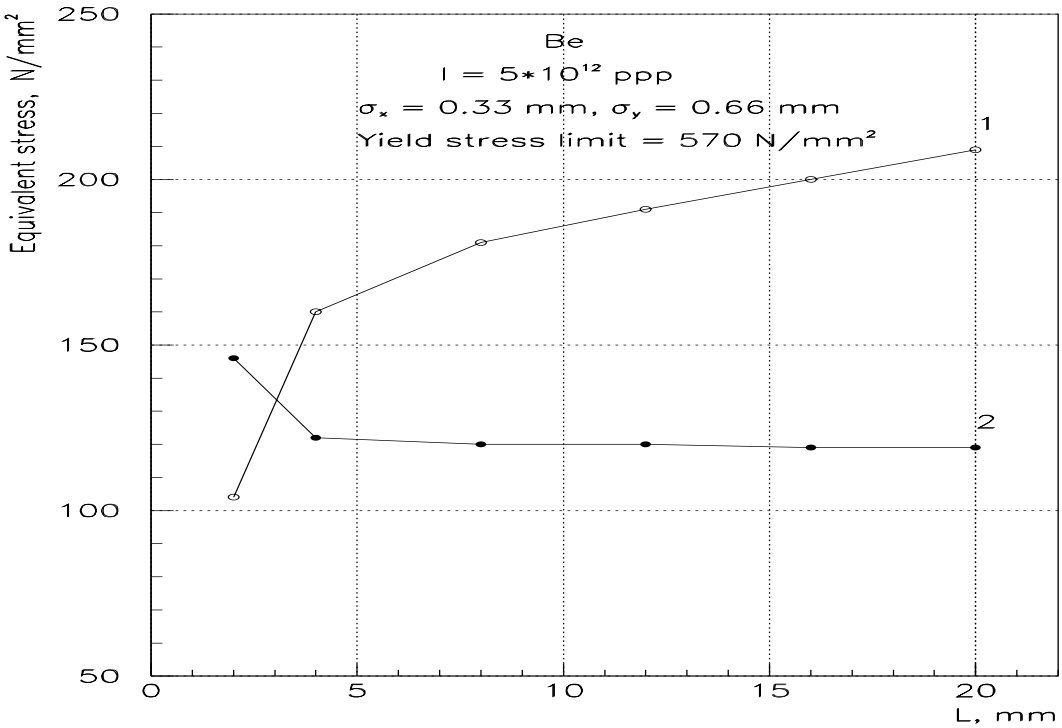

Figure 2.5: Equivalent stresses in the target prototype as a function of the subsegment length.

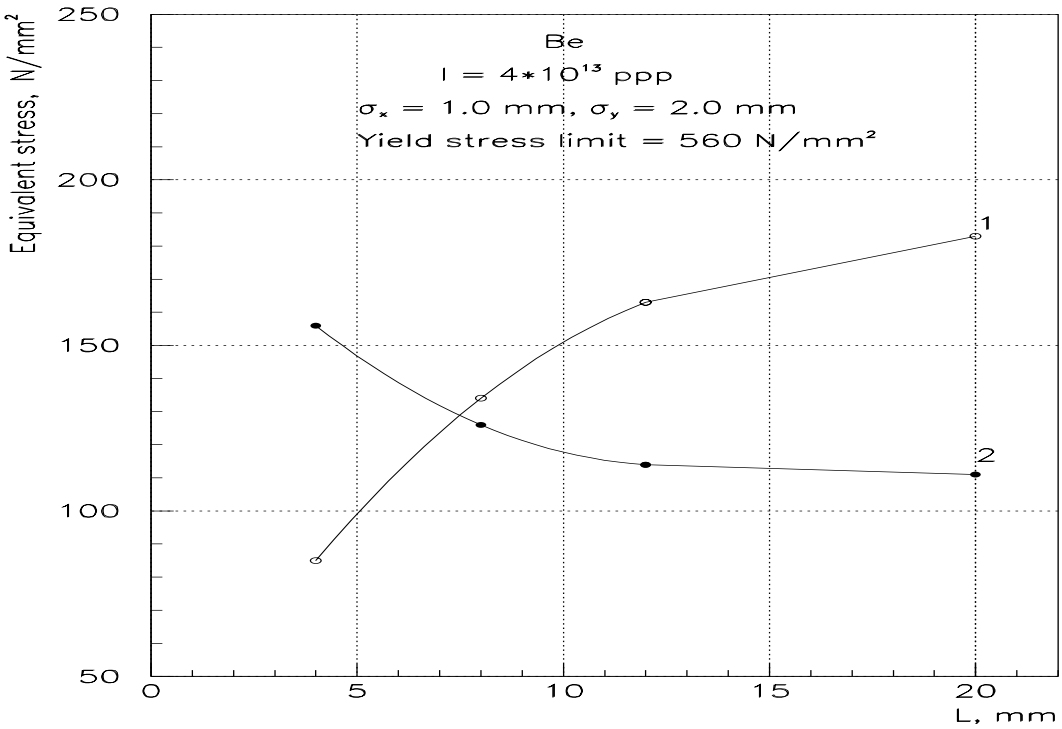

Figure 2.6: Equivalent stresses in the second segment of the full scale Be target as a function of the subsegment length.

References

[1] M.Reichanadter, Specification for the Design of the MI-40 Abort Core Box, (Engineering Specification 1451-ES-333047) Fermilab, Batavia, 1996.

[2] M.Reichanadter, C.M.Bhat, C.Crawford, P.S.Martin, A High Intensity Beam Absorber Corebox for the Fermilab Main Injector Abort System, Fermilab, Batavia, 1996.

[3] I.Azhgirey et al, Proc. XV Conference on Charged Particles Accelerators, p.74, Protvino, 1996.

[4] A.Abramov et al, IHEP Preprint 84-64, Serpukhov, 1984.

[5] N.Mokhov, FERMILAB-TM-628, Batavia, 1995.